Combustion Science and Technology
Publication details, including instructions for authors and subscription information:
http://www.tandfonline.com/loi/gcst20

A numerical analysis of ignition to steady downward flame spread over a thin solid fuel

Kuo-Kuang Wu [a] & Chiun-Hsun Chen [a]
[a] Department of Mechanical Engineering , National Chiao-Tung University , HsinChu, Taiwan, R.O.C.
Published online: 17 Sep 2010.

To cite this article: Kuo-Kuang Wu & Chiun-Hsun Chen (2003) A numerical analysis of ignition to steady downward flame spread over a thin solid fuel, Combustion Science and Technology, 175:5, 933-964, DOI: 10.1080/00102200302408

To link to this article: http://dx.doi.org/10.1080/00102200302408

Combust. Sci. and Tech., 175: 933–964, 2003

0010-2203/03 $12.00 + .00
DOI: 10.1080/00102200390206933

Taylor & Francis
Taylor & Francis Group

A NUMERICAL ANALYSIS OF IGNITION TO STEADY DOWNWARD FLAME SPREAD OVER A THIN SOLID FUEL

KUO-KUANG WU AND CHIUN-HSUN CHEN*

Department of Mechanical Engineering,
National Chiao-Tung University, HsinChu, Taiwan, R.O.C.

A numerical analysis using an unsteady combustion model is presented to study the ignition and subsequent downward flame spread over a thermally thin solid fuel in a gravitational field. The solid-fuel temperature rises gradually in the heat-up stage and the pyrolysis becomes more intense. Ignition, including the induction period and thermal runaway, occurs as soon as a flammable mixture is formed and the gas-phase temperature, heated by the solid fuel, becomes high enough. During the induction period, the reactivity and temperature in the gas phase are mutually supportive. The thermal runaway consists of a burning premixed flame as the flow moves with the flame front. This is followed by a transition from a premixed flame into a diffusion flame. The flame front extends along and toward the upstream virgin fuel as the diffusion flame is formed. Finally, steady flame spread takes place as burnout appears. The ignition delay time is found to be controlled mainly by the time required to form the flammable mixture and is almost independent of the gravity level and the ambient oxygen index. The ignition delay time increases nearly linearly with an increase in solid-fuel thickness within the range of $0.005\,\text{cm} \leqslant \bar{\tau} \leqslant 0.02\,\text{cm}$ and is proportional to $(\bar{Q}_{\max})^{-1.11}$ within $2\,\text{W/cm}^2 \leqslant \bar{Q}_{\max} \leqslant 8\,\text{W/cm}^2$. The steady downward flame-spread rate decreases with increases in the gravity level or fuel thickness and with decreases in the ambient oxygen index but is independent of the incident peak heat flux. The blowoff limit is around $6.7\,\bar{g}_e$ and the extinction limit is found to be $Y_{O\infty} = 0.131$.

Received 9 July 2002; accepted 3 December 2002.

The authors would like to thank the National Science Council of the Republic of China for financially supporting this research under Contract no. NSC89-2212-E-009-049.

*Address correspondence to chchen@mail.nctu.edu.tw

Keywords: downward flame, ignition, gravity, fuel thickness, oxygen index, incident peak heat flux

INTRODUCTION

Theoretical analyses of downward flame spread over thin solid fuels in gravitational fields have been carried out by Chen and coworkers (Chen and Cheng, 1994; Chen and Hou, 1991; Duh and Chen, 1991; Lin and Chen, 1999a). They applied a steady combustion model to predict the flame-spread rate at different gravity levels. Generally, the flame-spread rate was found to decrease gradually as the gravity level increased. Blow-off at a high gravity level was identified. The radiation effect played a more important role in lower gravity regimes, where $\bar{g}/\bar{g}_e < 1$. The flame temperature decreases by radiation heat loss. The solid fuel receives energy from the flame, which simultaneously decreases so that it cannot pyrolyze sufficient fuel to sustain flame spread. As the critical limit is reached, the flame extinguishes; this is called radiation extinction.

A steady combustion model cannot exhibit ignition over a solid surface. Therefore, an unsteady combustion model is necessary to simulate the flame development process from ignition to flame spread. A time-dependent solution will eventually reach a steady flame-spread rate, if it exists, which should equal the rate obtained by the steady combustion model. Even if no steady flame-spread solution exists, the unsteady model provides a correct solution. A steady-state model cannot guarantee an accurate solution.

Tewarson and Ogden (1992) experimentally investigated how long it would take for ignition to occur by varying the external heat flux $\bar{q}_{ex}$ (10–60 kW/m^2) under natural and coflow conditions for horizontal PMMA samples. Their results indicated that under the critical heat flux value ($\bar{q}_{cr}$), there is no ignition. If the external heat flux is greater than $\bar{q}_{cr}$, then the ignition delay time t_{ig} decreases as $\bar{q}_{ex}$ increases. Kashiwagi et al. (1996) studied flame-spread behaviors over thermally thin cellulosic samples. Their experiments were conducted using a lamp as an external radiant source in a 50% oxygen atmosphere under three different wind velocities in a 10-s drop tower. The results showed that there were no significant influences on the ignition delay time of the slow wind (0–5 cm/s). The propagation speed in the upstream direction increased with the imposed flow stream while the propagation speed in the downstream direction decreased.

A similar experiment performed by McGrattan et al. (1996) used a thermally thin cellulosic sheet, heated by an external thermal radiation source, in the 2.2-s NASA drop tower. The wind velocity range was the same as that used in Kashiwagi et al.'s (1996) experiments. They also developed a two-dimensional time-dependent model to predict the ignition and transition to flame spread. Both the experimental and calculated results showed that with a slow, imposed wind, the upstream flame front is stronger and slightly faster than the quiescent counterpart due to a greater oxygen supply. However, the downstream flame front tends to extinguish. This is caused by the "oxygen shadow" cast by the upstream flame. The ignition delay time depends mainly on the peak external radiation flux, whereas the transition to steady-state flame spread depends mainly on the broadness of the flux distribution. The broader the radiative flux distribution, the greater the transient flame-spread rate due to the preheating of the sample ahead of the flame front by the external radiation; thus, the greater the delay to steady-state flame spread.

A computational model of three-dimensional time-dependent flame spread over a thermally thin cellulosic sheet in a microgravity environment was presented by Jiang and Fan (1995). This model predicted the flame spread over a horizontal solid fuel in a slow forced flow under a gravitational field and the flame spread in a quiescent environment in an enclosed chamber under gravitational acceleration, parallel to the fuel surface. Because it was assumed that ignition takes place at $\bar{t} = 0$ s, the flame structures and temperature distributions were limited after ignition. Therefore, it was impossible to describe flame behavior prior to flame ignition.

Nakabe et al. (1994) developed an axisymmetric, time-dependent model to describe autoignition and subsequent transition to flame spread over a thermally thin cellulosic sheet heated by an external radiation in a quiescent microgravity environment. This work found that autoignition occurs for 30% oxygen concentrations, but the transition to the flame spread does not occur until the oxygen concentration approaches 50%. Olson et al. (2001) experimentally studied the radiative ignition and transition to flame spread over thin cellulose fuel samples in a microgravity environment. The results indicated that the ignition delay time is proportional to the gas-phase mixing time, which is estimated by using the inverse flow rate. The ignition delay time is affected strongly by flow velocity at lower oxygen concentrations. Moreover, they found that the ignition occurs in a quiescent atmosphere environment, but the flame is quickly extinguished.

Altenkirch et al. (1980) experimentally investigated buoyancy effects on downward flame spread over thermally thin fuels. Parameter variation was accomplished by performing the flame-spread experiments in a closed chamber, swung on a centrifuge, to generate elevated gravitational accelerations. They found that an increase in the buoyancy level caused the flame-spread rate to drop until no propagation was possible. This indicates that an increasing gravity level tends to increase induced flow intensity such that it retards downward flame spread. Later, Sacksteder and T'ien (1994) examined flame spread in partial gravity accelerations ranging from 0.05 to $0.6\bar{g}_e$ using aircraft tests to cover regimes not previously explored. Combined with the centrifuge data in elevated gravity, the results showed a nonmonotonic spread rate variation with gravitational acceleration, implying that certain controlling mechanisms, such as radiation, may become crucial in low-gravity regimes.

Di Blasi (1994, 1995) studied the solid-fuel thickness influence on flame spread. Three main limits of flame spread were identified. In the first, where the fuels are very thin, the flame-spread rate increases with the solid-fuel thickness. For the second, the fuels are thin, and the flame-spread rate starts to decrease as the solid fuel becomes thicker. The flame-spread rate becomes nearly constant in the third category, thick fuels. Lastrina et al. (1971) investigated the dependence of the flame-spread rate on the fuel-bed thickness for polymeric and cellulosic materials. They found that the flame-spread rate varied inversely with the fuel-bed thickness for thin fuels. For specimens thicker than 0.06 in., the flame-spread rate was less sensitive to thickness. Suzuki et al. (1994) performed a series of downward flame-spread experiments over paper sheets from 0.4 to 10 mm thickness under natural-convective conditions. A sample sheet was clamped between pairs of metal straps at both sides without limiting the air supply. A slit burner was used as an ignition source to ignite the sample at its top edge. Experimental results indicated that the sample thickness according to the corresponding flame behaviors can be classified into four types: (1) thermally thin, (2) thermally thick, (3) unstable, and (4) extinction region.

Lin and Chen (1999b) numerically studied how the external radiant peak heat flux and oxygen concentration affected the ignition delay time for downward flame spread. The predicted results showed that the ignition delay time decreases as the radiant peak heat flux or oxygen concentration increases. They also found that the ignition delay time is independent of the oxygen concentration when the radiant peak heat flux

is greater than $6\,W/cm^2$. If the radiant peak heat flux is lower than a critical value, ignition does not occur. Mikkola and Wichman (1989) developed a theoretical model to predict the ignition delay time using an energy balance. They concluded that the ignition delay time was inversely proportional to the peak external heat flux [$t_{ig} \propto (\bar{Q}_{max})^{-1}$], for a thermally thin fuel [$t_{ig} \propto (\bar{Q}_{max})^{-2}$], and for an intermediate-thickness fuel [$t_{ig} \propto (\bar{Q}_{max})^{-\frac{1}{2}}$].

Several experiments and models, such as those by Fernandez-Pello and Hirano (1983), Chen and Hou (1991), Olson (1987, 1991), and Sacksteder and T'ien (1994), indicated that the ambient oxygen concentration will alter flame behavior. In summary, the flame-spread rate increases with the ambient oxygen concentration and if this concentration is lower than a critical value, the flame will extinguish.

From the preceding literature review, very few works considered the complete flame-development process from ignition to subsequent flame spread in normal gravity. The main purpose of this work is to simulate the ignition of a vertical thin cellulosic fuel, subjected to an external radiant flux, and the transition to a steady downward flame spread in a naturally convective environment. A series of gas-phase temperature contours combined with the flow velocity vector distribution, fuel/oxidizer concentration, and so on, will be given and discussed in detail to understand the process. This discussion is followed by a parametric study, in which the gravity level, fuel thickness, oxygen index, and incident peak heat flux were changed. The flame behaviors are quantified through the ignition delay time and the steady flame-spread rate. The predicted results are compared with experimental measurements and relevant numerical studies.

MATHEMATICAL MODEL

The problem configuration is shown in Figure 1. The solid fuel is ignited at the tip by an external radiant heat flux. After ignition, a flame is initiated at the tip and propagates downward. An induced flow, existing ahead of the flame front, is driven upward by buoyancy. The coordinate system is fixed at the tip point ($x = y = 0$) of the solid fuel. The corresponding assumptions and normalization procedure can be found in Lin and Chen (1999b) and are not represented here for brevity. The nondimensional governing equations for both the gas and solid phase are

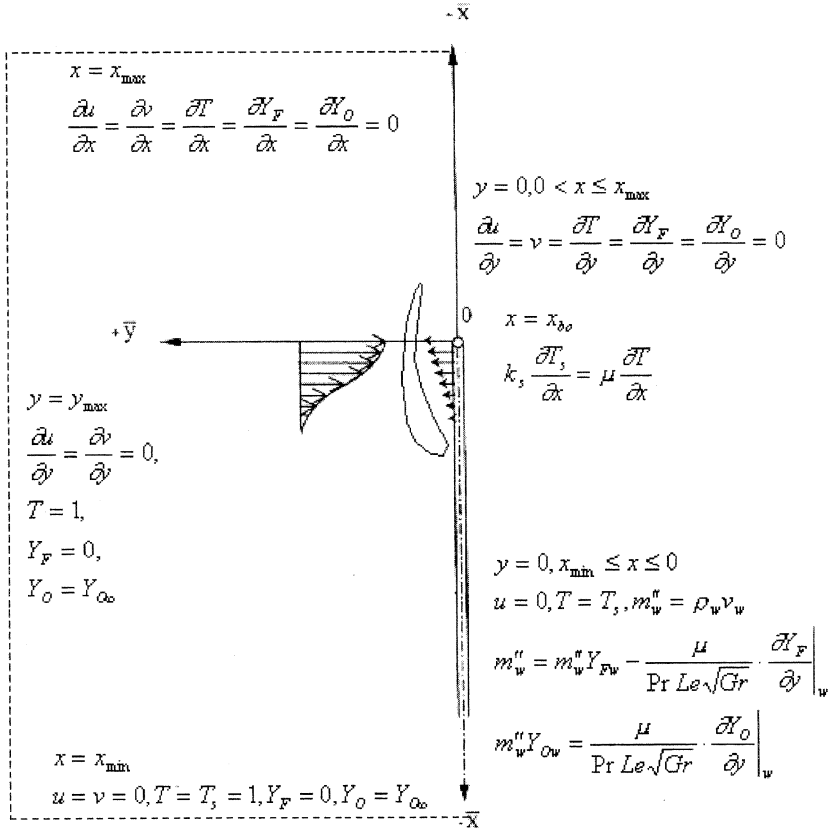

Figure 1. A schematic illustration of radiative ignition over a vertical solid fuel.

shown in Table 1, for which notation is defined in the nomenclature. Figure 1 presents the boundary conditions, which are initially as follows, for gas phase:

$$t \le 0 \qquad u = 0 \qquad v = 0 \qquad T = 1 \qquad Y_F = 0 \qquad Y_O = Y_{O\infty} \tag{1}$$

and for solid phase:

$$t \le 0 \qquad \rho_s = 1 \qquad T_s = 1 \tag{2}$$

This model is solved with a marching time step. At each time step, the gas- and solid-phase equations are solved separately. Iteration is

Table 1. Nondimensional governing equations

	Gas-phase governing equation		
	$\frac{\partial}{\partial t}(\rho\phi)+\frac{\partial}{\partial x}(\rho u\phi)+\frac{\partial}{\partial y}(\rho v\phi)=\left[\frac{\partial}{\partial x}\left(\Gamma\frac{\partial\phi}{\partial x}\right)+\frac{\partial}{\partial y}\left(\Gamma\frac{\partial\phi}{\partial y}\right)\right]+S$		
Equation	ϕ	Γ	S
Continuity	1	—	0
x-Momentum	u	$\frac{\mu}{\sqrt{Gr}}$	$-\frac{\partial p}{\partial x}+S_u+\frac{\rho_\infty-\rho}{\rho_\infty-\rho_f}$
y-Momentum	v	$\frac{\mu}{\sqrt{Gr}}$	$-\frac{\partial p}{\partial y}+S_v$
Energy	T	$\frac{\mu}{Pr\sqrt{Gr}}$	$-q\dot{\omega}_F$
Fuel	Y_F	$\frac{\mu}{PrLe\sqrt{Gr}}$	$\dot{\omega}_F$
Oxidizer	Y_O	$\frac{\mu}{PrLe\sqrt{Gr}}$	$f\dot{\omega}_F$
	Solid-phase governing equations		
Mass	$m_s''=-\frac{d\rho_s}{dt}=A_s\rho_s\exp(-\frac{E_s}{T_s})$		
Energy	$\rho_s\frac{\partial T_s}{\partial t}=\alpha_s\frac{\partial^2 T_s}{\partial x^2}+m_s''[L+(1-C)(T_s-1)]+\frac{\mu}{\tau Pr\sqrt{Gr}}\frac{\partial T}{\partial y}\Big\vert_w+q_{ex}$		

Where

$$S_u=\frac{1}{3}\frac{\partial}{\partial x}\left(\frac{\mu}{\sqrt{Gr}}\frac{\partial u}{\partial x}\right)+\frac{\partial}{\partial y}\left(\frac{\mu}{\sqrt{Gr}}\frac{\partial v}{\partial x}\right)-\frac{2}{3}\frac{\partial}{\partial x}\left(\frac{\mu}{\sqrt{Gr}}\frac{\partial v}{\partial y}\right)$$

$$S_v=\frac{1}{3}\frac{\partial}{\partial y}\left(\frac{\mu}{\sqrt{Gr}}\frac{\partial v}{\partial y}\right)+\frac{\partial}{\partial x}\left(\frac{\mu}{\sqrt{Gr}}\frac{\partial u}{\partial y}\right)-\frac{2}{3}\frac{\partial}{\partial y}\left(\frac{\mu}{\sqrt{Gr}}\frac{\partial u}{\partial x}\right)$$

$\dot{\omega}_F=-Da\,\rho^2 Y_F Y_O\exp(-E/T)$

Equation of state: $\rho\cong\frac{\gamma}{T}$

The equation for viscosity variation with temperature: $\mu=\frac{T}{\gamma}$

Table 2. Grid and time-step test results

Grid number $x \times y$	Time step (s)	Ignition delay time (s)
184×40	0.027	0.5477
184×80	0.027	0.5477
224×40	0.027	0.5477
284×40	0.027	0.5477
184×40	0.0027	0.5395
184×40	0.081	0.5751

performed until all variables converge within acceptable criteria. Following this, we march to the next time step.

By assuming that the surface reflectivity is null and neglecting the attenuation on the surface temperature effect, the numerical calculation is initiated from a prescribed external radiant heat flux, q_{ex}, input on the fuel surface at time $t = 0$. The profile of the incident radiation flux is a half Gaussian distribution, in which the half-width is 0.5 cm with a peak value of $5\,W/cm^2$ aimed at the origin of coordinates. The nondimensional external radiation flux is

$$q_{ex} = Q_{ex} \exp(-\beta x^2) \tag{3}$$

When the solid reaches burnout the char is removed by the gravitational effect. As a consequence, the tip of the solid fuel (x_{bo}) moves. Because of this, the moving boundary conditions for the solid phase appear in the model.

The numerical scheme adopts the SIMPLE algorithm (Patankar, 1980). The grid-independent test results are shown in Table 2. Here this study selected the nondimensional time step of $\Delta t = 5$ (equivalent to real time 0.027 s) and the nonuniform grid distribution of 184×40 by considering the optimization between the solution resolution and the requirements for computational time and memory space. The computation was performed on a PC.

RESULTS AND DISCUSSION

In this section, the entire flame-development process will be depicted in detail using a reference case. The conditions are as follows: solid fuel

Table 3. Gas and solid properties values

Symbol	Units	Value
$\bar{E}_s$	J/mol	1.255×10^5
$\bar{A}_s$	l/s	5×10^{10}
$\bar{L}$	J/g	-753
$\bar{k}_s$	W/cm K	1.255×10^{-3}
$\bar{C}_s$	J/g K	1.26
$\bar{\rho}_{s_\infty}$	g/cm^3	0.75
$\bar{\alpha}_s$	cm^2/s	1.328×10^{-3}
$\bar{T}_v$	K	618
f	—	1.185
$\bar{R}$	J/mol K	8.314
$\overline{C}_p$	J/g K	$f(\bar{T}^*)$
$Y_{O\infty}$	—	0.233
$\overline{\rho}^*$	g/cm^3	$f(\bar{T}^*)$
$\bar{q}$	J/g	1.674×10^4
$\overline{\alpha}^*$	cm^2/s	$f(\bar{T}^*)$
$\overline{T}_\infty$	K	298
$\overline{T}^*$	K	1570
$\overline{k}^*$	W/cm K	$f(\bar{T}^*)$
$\overline{\mu}^*$	g/cm s	$f(\bar{T}^*)$
$\bar{E}$	J/mol	8.720×10^4
$\bar{B}$	cm^3/mols	1.00×10^{12}
$\bar{\tau}$	cm	0.0098

half-thickness was 0.0098 cm; ambient oxygen index, 0.233; ambient gravitation. The thermophysical properties are listed in Table 3. The important nondimensional parameters are summarized in Table 4. The detailed presentation is shown in Figures 2–6.

Radiative Ignition Process

Figure 2 shows the solid-fuel temperature and density histories from $\bar{t} = 0$ to $\bar{t} = 2.87$ s, the first appearance of burnout. At $\bar{t} = 0$, the incident radiation flux of the half Gaussian distribution is imposed. The solid fuel absorbs the heat and raises its temperature. This heat-up is sustained to $\bar{t} = 0.55$ s, the starting point of gas-phase ignition. From Figure 2(*a*), the increase in the solid temperature is limited to $x \geq -8$ in this time period. The half-width of the incident heat flux distribution, -3.6, is apparent in the heat-conduction effect in the solid. The solid temperature profile is

Table 4. Nondimensional parameters

Symbol	Parameter group	Value
Pr	$\bar{\nu}/\bar{\alpha}$	0.702
Le	$\bar{\alpha}/\bar{\mathbf{D}}$	1.000
Gr	$\bar{g}(\bar{\rho}_\infty - \bar{\rho}_\mathrm{f})\bar{\delta}^3/\bar{\rho}^*\bar{\nu}^{*2}$	Variable
Da	$\bar{B}\bar{\rho}^*\bar{\delta}/\bar{V}_\mathrm{r}$	Variable
C	$\overline{C}_p/\overline{C}_\mathrm{s}$	0.986
γ	$\overline{\mathrm{T}}^*/\overline{\mathrm{T}}_\infty$	Variable
T_V	$\overline{\mathrm{T}}_\mathrm{v}/\overline{\mathrm{T}}_\infty$	2.07
E	$\bar{\mathrm{E}}/\bar{\mathrm{R}}\bar{\mathrm{T}}_\infty$	35.196
q	$\bar{q}/\overline{C}_p\overline{T}_\infty$	45.224
ρ_sf	$\overline{\rho}_\mathrm{sf}/\overline{\rho}_{\mathrm{s}\infty}$	0.070
k_S	$\overline{k}_\mathrm{s}/\overline{k}^*$	Variable
L	$\bar{L}/\overline{C}_\mathrm{s}\overline{T}_\infty$	-2.005
A_s	$\bar{A}_\mathrm{s}\bar{\alpha}^*/\bar{V}_\mathrm{r}^2$	Variable
E_s	$\bar{E}_\mathrm{s}/\overline{R}\,\overline{T}_\infty$	50.654
τ	$\bar{\tau}\bar{C}_\mathrm{s}\bar{\rho}_{\mathrm{s}\infty}\bar{V}_\mathrm{r}/\bar{k}^*$	Variable
α_s	$\bar{\alpha}_\mathrm{s}/\bar{\alpha}^*$	Variable

taken to be a bell shape. The peak is not exactly at $x = 0$ but is slightly shifted because the solid-fuel tip can simultaneously transfer heat to the ambient air as it receives the energy from the input heat flux. In this time interval, the solid fuel only generates a small amount of fuel vapor, as shown in Figure 2(*b*).

Figure 3 shows the maximum temperature time history for the entire field, including both the gas and solid phases. The maximum temperature occurs at the solid phase in the heat-up stage and induction period ($0\,\mathrm{s} < \bar{t} \leq 0.71\,\mathrm{s}$). The solid fuel transfers heat to the adjacent gas layer via conduction and raises its temperature. The temperature difference between the solid and gas phases increases with time in the heat-up stage ($\bar{t} \leq 0.55\,\mathrm{s}$). In the induction period ($0.55\,\mathrm{s} < \bar{t} \leq 0.71\,\mathrm{s}$) the solid-phase temperature raise rate slows down. This is because the absorption energy is used to raise the solid-phase temperature in the heat-up stage but part of the absorption energy is used ot pyrolyze the fuel vapors released in the induction period. This phenomenon is the same as in experiments (Kashiwagi, 1982) for PMMA and red oak. Although these two fuels are thick, the phenomena are also expected for thin fuels. Figure 4(*a*) shows the isotherm distribution in the gas phase at the end of heat-up, $\bar{t} = 0.55\,\mathrm{s}$. The temperature is lower than in the solid phase, Figure 2(*a*).

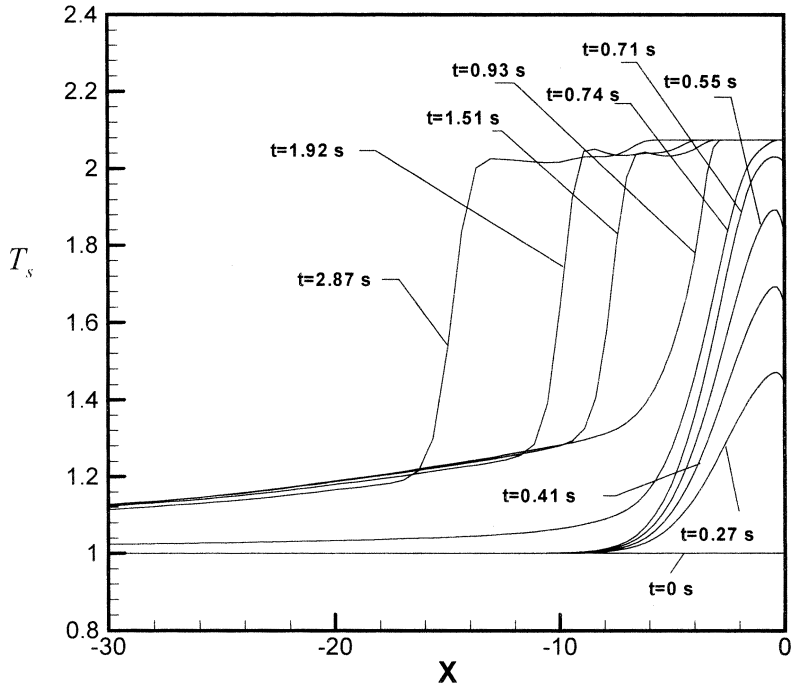

Figure 2(*a*). Change of solid-phase temperature distribution with time.

The thermal plume downstream is a little longer because of the induced flow.

We define the gas-phase ignition as occurring as soon as its dimensional reaction rate ($\overline{\dot{\omega}}_F$) reaches 10^{-4} g/cm^3 s, according to Nakabe et al. (1994) and Ferkul and T'ien (1994). In the former reference (Nakamura et al., 2000), they discussed the effects of ignition criteria and also suggested the same ignition criterion. At $\bar{t} = 0.55$ s, the first appearance of $(\overline{\dot{\omega}}_F) = 10^{-4}$ g/cm^3 s develops near the tip and ignition starts to occur. An extra source for the gas-phase temperature rise is from the chemical reaction in addition to the solid. The gas-phase temperature rises between $\bar{t} = 0.55$ and 0.71 s, but it is still lower than the solid-phase temperature (Figure 3), indicating that the chemical reaction is so weak that it does not yet contribute. In the meantime, the solid pyrolysis becomes intense, see Figure 2(*b*), leading to the formation of a flammable mixture near the solid fuel. Increased pyrolysis makes the gas-phase chemical reaction rate increase as well.

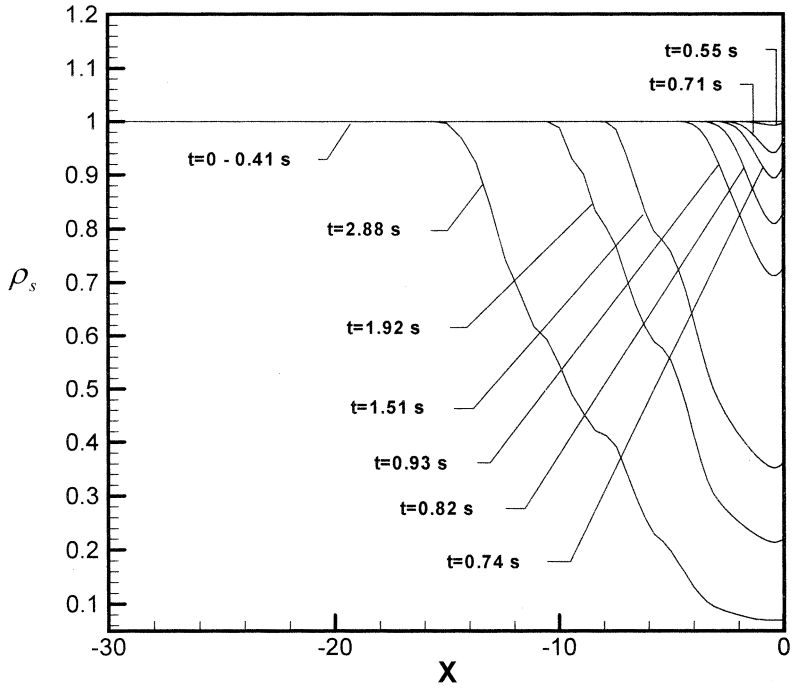

Figure 2(*b*). Change of solid-phase density distribution with time.

The fuel vapor and oxidant are now well mixed by diffusion and convection, forming a flammable mixture, Figures 5(*a*) and 5(*b*). However, the gas-phase temperature, Figures 4(*a*) and 4(*b*), is not high enough to activate the chemical reaction. The induced flow velocity is not high either; for example, the maximum nondimensional velocity is about 1.277 at $\bar{t} = 0.71$ s. By the way, Figures 4 and 5 are illustrated in nondimensional form and do not present the full computational region. Only the domains of interest are displayed.

After that, the flame grows quickly within a very short period, $0.71\,\text{s} \leq \bar{t} \leq 0.74\,\text{s}$, Figures 4(*b*) and 4(*c*), which is the development of a premixed flame. The outward velocity vectors, as shown in Figure 4(*c*), indicating that the flow is moving with the flame front, also characterize this. The chemical reaction rate increases sharply and releases much heat because the flammable mixture simultaneously burns out. This process is illustrated in Figures 5(*b*) and 5(*c*). In Figure 2(*a*), the maximum

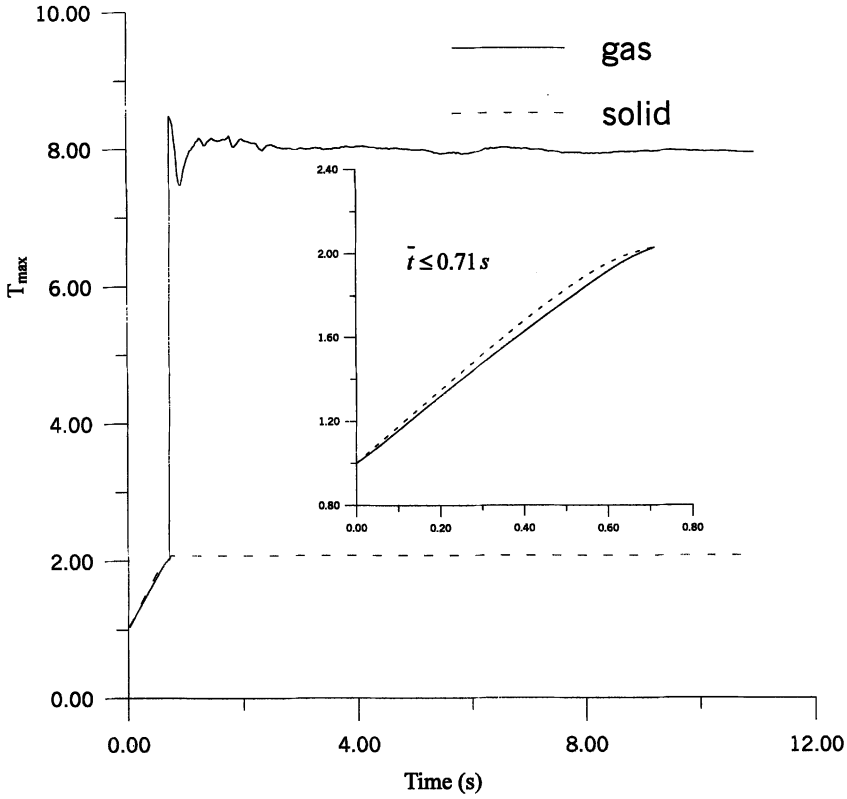

Figure 3. Time history of maximum temperature for solid and gas phases.

solid-fuel temperature starts to reach the pyrolysis temperature ($T_s = 2.07$) at $\bar{t} = 0.74$ s and then maintains this temperature; however, burnout does not yet occur, see Figure 2(*b*). In Figure 3, the maximum gas-phase temperature increases from 2.03 to 8.49 within 0.03 s. This can be regarded as thermal runaway. The flame size reaches a maximum value at $\bar{t} = 0.74$ s. After that, the flame size reduces and the temperature drops to about 150 K and becomes constant ($T = 8$) afterward. This flame gradually becomes a diffusion flame.

After $\bar{t} > 0.74$ s, the flame begins to shrink. A transformation from a premixed flame into a diffusion flame can be seen from Figures 4(*c*)–(*f*). The flame size reduces and the velocity vectors are directed inward toward the high-temperature area. When the diffusion flame is formed

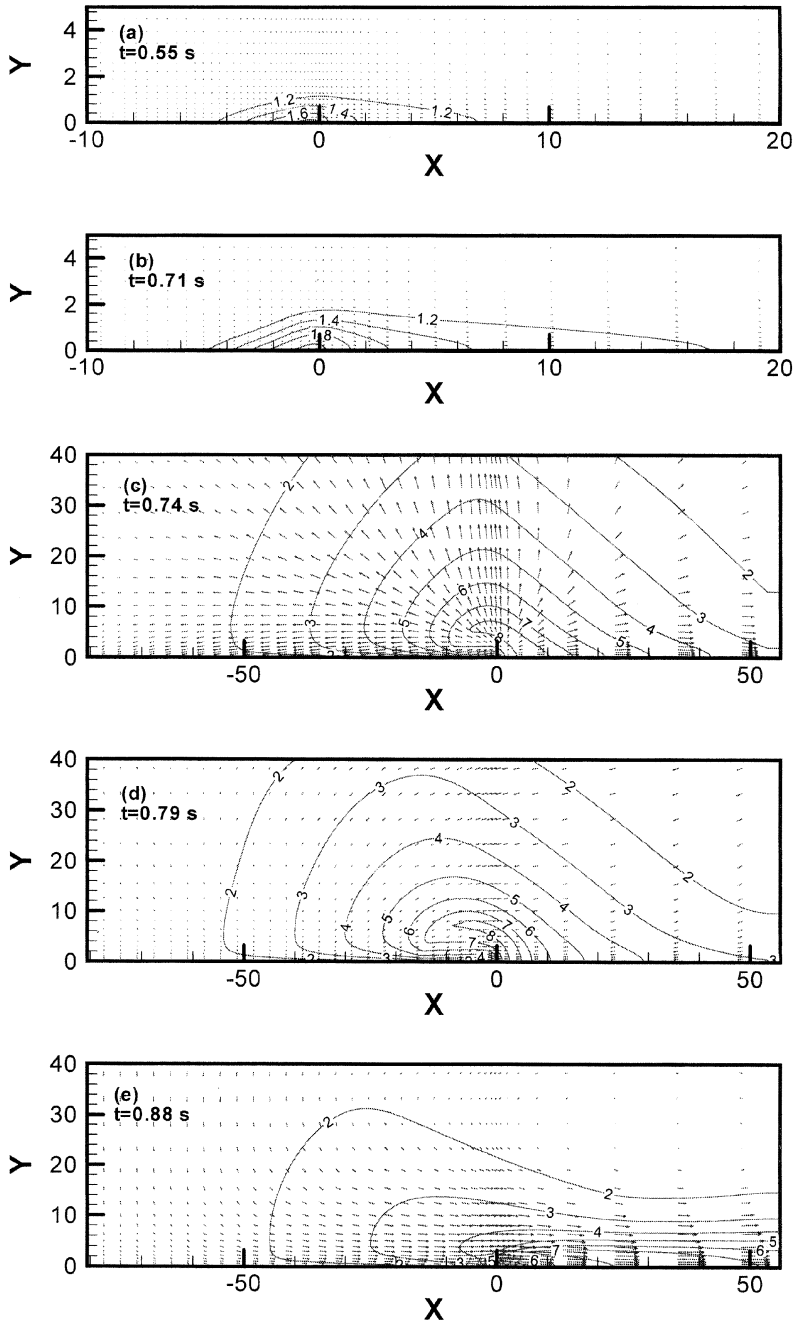

Figure 4. Isotherm and velocity vector distributions for (*a*) $t = 0.55$ s, (*b*) $t = 0.71$ s, (*c*) $t = 0.74$ s, (*d*) $t = 0.79$ s, (*e*) $t = 0.88$ s, (*f*) $t = 0.93$ s, (*g*) $t = 1.07$ s, (*h*) $t = 2.87$ s, and (*i*) $t = 10.95$ s.

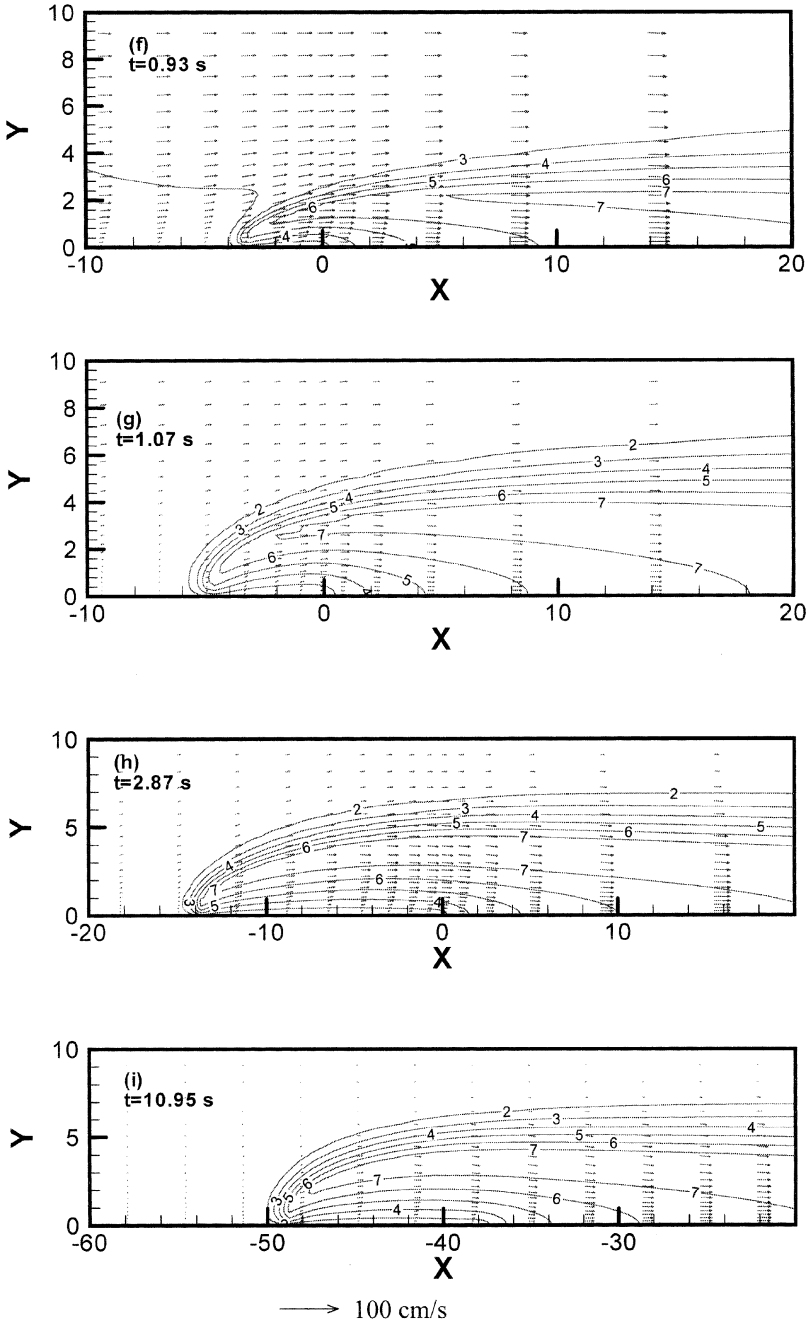

Figure 4. Continued.

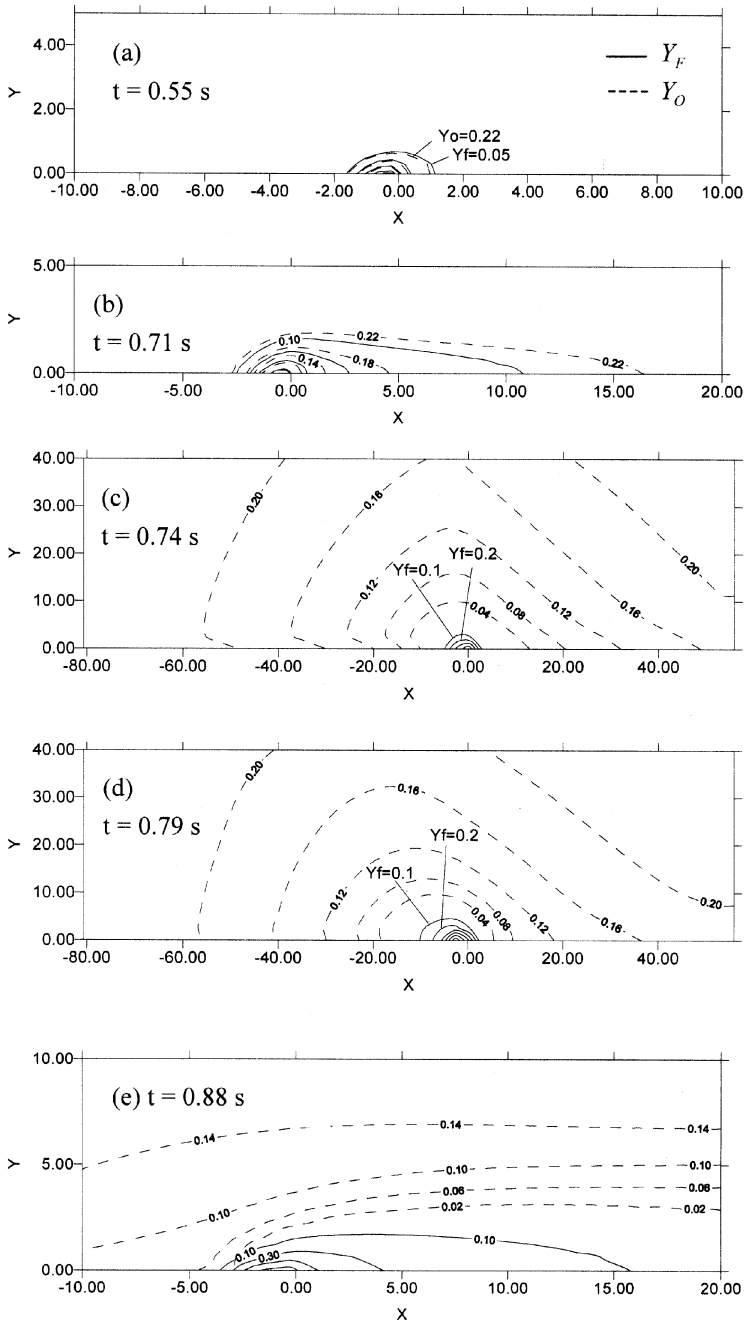

Figure 5. Fuel and oxidizer mass fraction contours for (*a*) $t = 0.55$ s, (*b*) $t = 0.71$ s, (*c*) $t = 0.74$ s, (*d*) $t = 0.79$ s, (*e*) $t = 0.88$ s, (*f*) $t = 0.93$ s, (*g*) $t = 1.07$ s, (*h*) $t = 2.87$ s, and (*i*) $t = 10.95$ s.

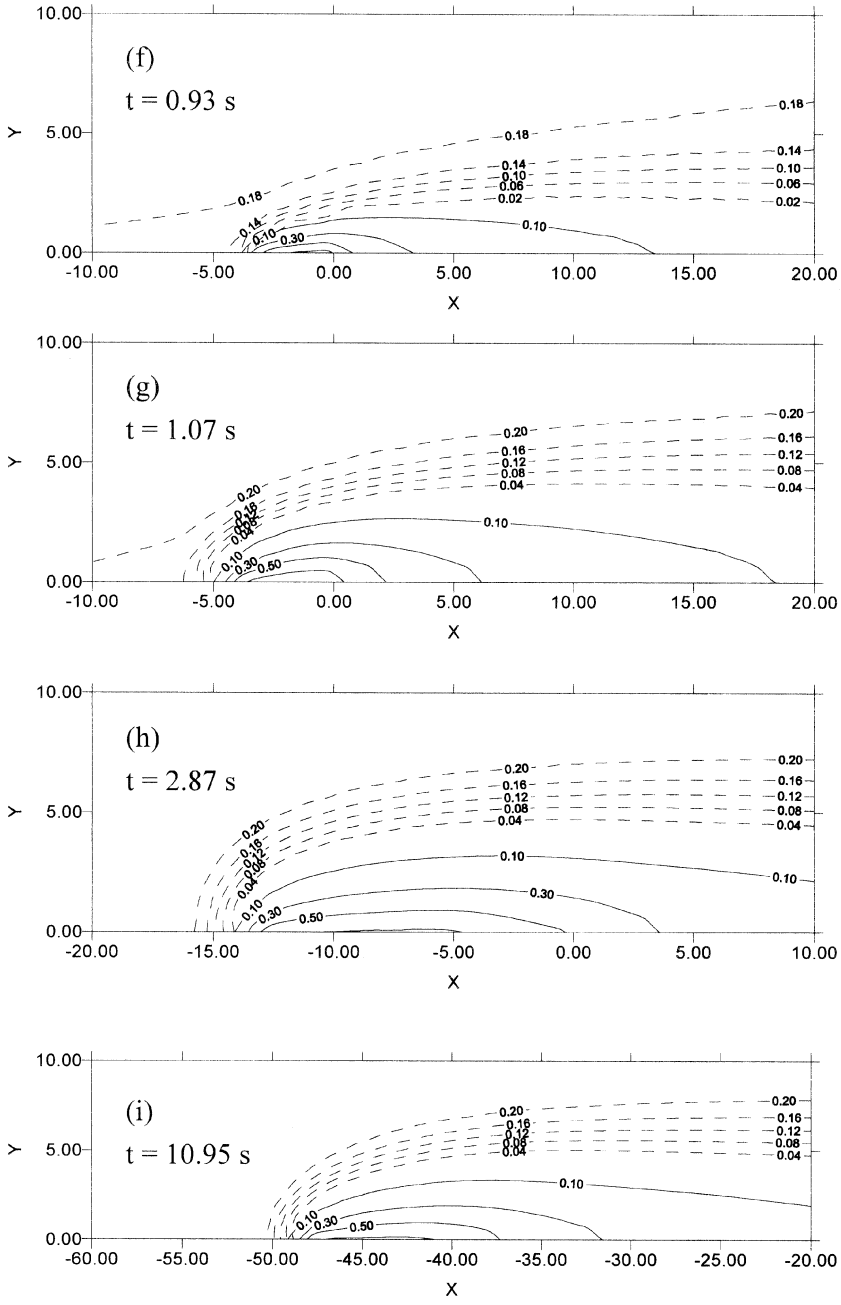

Figure 5. Continued.

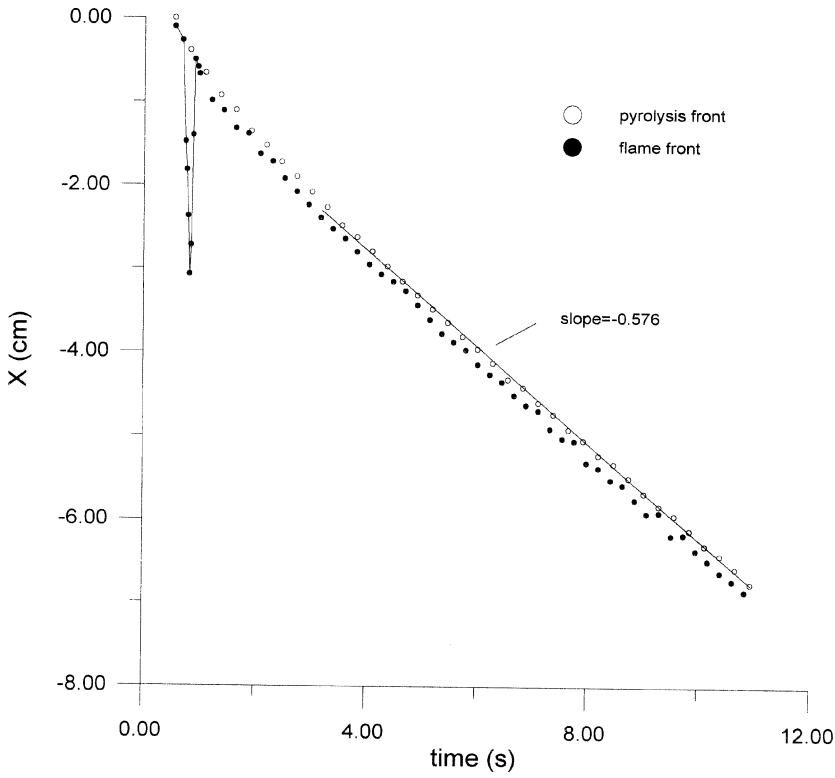

Figure 6. Flame front and pyrolysis front position vary with time.

around $\bar{t} = 0.93$ s, the main stream flows upward. Figures 5(*c*)–(*f*) show the corresponding evolution of the transition fuel and oxidizer mass fraction contours. From Figure 2, between $\bar{t} = 0.74$ and 0.93 s, the temperature at the region near the tip reaches the pyrolysis temperature, $T_s = 2.07$, but burnout does not yet occur.

When the flame becomes a diffusion flame, it requires fresh fuel vapors to support itself. The flame front extends upstream (downward direction) to further pyrolyze the solid fuel to generate vapors for a flammable mixture ahead of itself. Meanwhile, the flame preheats the incoming induced cold oxidizer flow to initiate the gas-phase reaction. This extension continues and the pyrolysis becomes more intense, Figure 2(*b*). Up to $\bar{t} = 2.87$ s, the burnout ($\rho_s = 0.07$) appears and the flame begins to spread downward. In this study, the char is removed at

burnout. The extension process in the gas phase can be seen in Figures 4(*f*)–(*h*). After that, the steady flame spread and the burnout point then move with the flame front. In the steady flame-spread process the flame appearance in Figure 4(*i*) is quite similar to that in Figure 4(*h*) within a time elapse of 8.08 s (from $\bar{t} = 2.87$ s to $\bar{t} = 10.95$ s).

Figure 6 depicts the flame front (the leading-edge contour of $\bar{\dot{\omega}} = 10^{-4}\,\mathrm{g/cm^3\,s}$) and pyrolysis front (the first upstream position of $\rho_s = 0.99$) positions as a function of time. After ignition ($\bar{t} = 0.55$ s), both the flame and pyrolysis fronts propagate continuously. The flame front is always slightly ahead of the pyrolysis front except for $0.74\,\mathrm{s} \leq \bar{t} \leq 0.88$ s, where the flame front is much farther in front of the pyrolysis front because of premixed flame thermal runaway burning. Experiment has shown that the flame front is slightly ahead of pyrolysis for thin cellulose materials (Parker, 1972). The steady flame-spread rate could be obtained from the slope of a best-fit line passing through the flame or pyrolysis front points in Figure 6. Although the steady flame-spread process can be identified after burnout occurs at $\bar{t} = 2.87$ s, the best-fit line initiates from $\bar{t} = 3.18$ s. A least-square technique was applied to draw a best-fit straight line past these points. According to this procedure, the resultant steady flame-spread rate was 0.576 cm/s with a standard deviation of 0.001 cm/s.

The Effects of Changing Gravity Level

The reference velocity was determined by equating the buoyancy and inertia forces to obtain the following expression:

$$\bar{V}_r = [\bar{g}(\bar{\rho}_\infty - \bar{\rho}_f)\bar{\alpha}^*/\bar{\rho}^*]^{\frac{1}{3}} \tag{4}$$

It is obvious that the reference velocity will change with $\bar{g}$. Therefore, nondimensional parameters such as Da, A_s, q_{ex}, and τ also vary with $\bar{g}$ (or reference velocity). Lowering Da, A_s, and q_{ex} corresponds to an increase of $\bar{g}$ but τ shows the opposite trend. The change in these parameters affects the gas-phase chemical reaction and solid-phase pyrolysis process.

The ignition delay times under different gravity levels, $0.5 \leq g \leq 6.7$, were found to be almost the same. This value is about 0.55 s and is explained as follows. From the previous section, the induced flow in the heat-up stage is small. Because of friction, the velocity is very small near

the sample surface for any incoming flow, either under induced or forced conditions. Therefore, flammable mixture is accumulated just above the pyrolysis region. Ignition takes place very close to the sample surface, and the ignition delay time is controlled mainly by the time to form the flammable mixture, not the induced incoming flow velocity. This can also be confirmed by the experiments of Kashiwagi et al. (1996), which showed that there are no significant effects of the slow wind on the ignition delay time, and by the experiments of Tewarson and Ogden (1992), which indicated that the ignition delay time is independent of the flow velocity.

Figure 7 illustrates the steady flame-spread rate under different gravity levels. The flame-spread rate decreases as $\bar{g}$ increases. The gas-phase conduction is the dominant mode of heat transfer for the downward (or opposed) flame spread over the thermally thin fuel. An increase in the induced flow by elevating $\bar{g}$ causes a reduction in the forward penetration of the conductive heat, leading to a lower flame-spread rate. This trend is the same as that obtained from the measurements of Altenkirch et al. (1980). On the other hand, de Ris' theory, (de Ris, 1969) predicted that flame-spread rate is independent of induced flow for thermally thin fuel. In other words, this theory indicates that there is no gravity effect on the flame spread over a thin fuel. The blowoff limit is around $g = 6.7$. Actually, the ignition fails at that level; therefore, it is impossible to have a subsequent spreading flame. The blowoff phenomenon is qualitatively consistent with the experiments of Altenkirch et al. (1980). However, the blowoff limit predicted using this model is greater than in Altenkirch et al. (1980). A possible reason is that the one-step overall chemical reaction used in this model may not be appropriate near the extinction limit. On the other hand, the flame spread increases with a decrease in gravity, which contradicts the experimental observations of Olson et al. (1988). This model does not consider radiation, which becomes crucial in low gravity (Chen and Cheng, 1994; Lin and Chen, 1999a).

The Effects of Changing Solid-Fuel Thickness

Varying $\bar{\tau}$ will directly affect the solid-phase heat transfer. Figure 8 displays the ignition delay time as a function of $\bar{\tau}$. It can be seen that the ignition delay time increases nearly linearly with an increase in solid-fuel thickness in the range of $0.005\,\text{cm} \leq \bar{\tau} \leq 0.02\,\text{cm}$. Since the thicker fuel

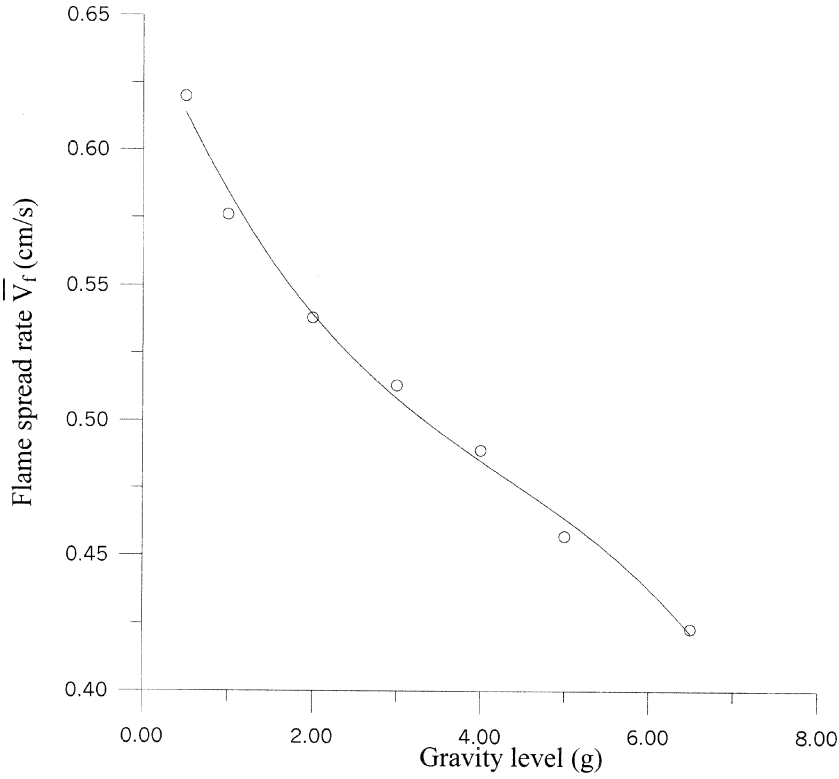

Figure 7. Steady flame-spread rate under different gravity levels.

needs more time to raise its temperature to form vapor, the ignition time for thicker fuel becomes longer, as expected.

Figure 9 reports the flame-spread rates, as a function of the fuel half-thickness, predicted by this numerical model, the thermal theory of de Ris (1969), and the work of Delichatsios (1986), respectively. For thin fuels, the de Ris theory predicts

$$\bar{V}_f = C\frac{\bar{k}}{\bar{\rho}_s \bar{C}_s \bar{\tau}}\left(\frac{\bar{T}_f - \bar{T}_V}{\bar{T}_V - \bar{T}_\infty}\right) \tag{5}$$

where C is a constant. Delichatsios (1986) demonstrates that the value of C is $\pi/4$. The other parameter values used in Eq. (5) are $\bar{k} = 9.838 \times 10^{-4}$ W/cm K, $\bar{\rho}_s = 0.75$ g/cm^3, $\bar{C}_s = 1.26$ J/g K, $\bar{T}_f = 2840$ K, $\bar{T}_V = 618$ K, and

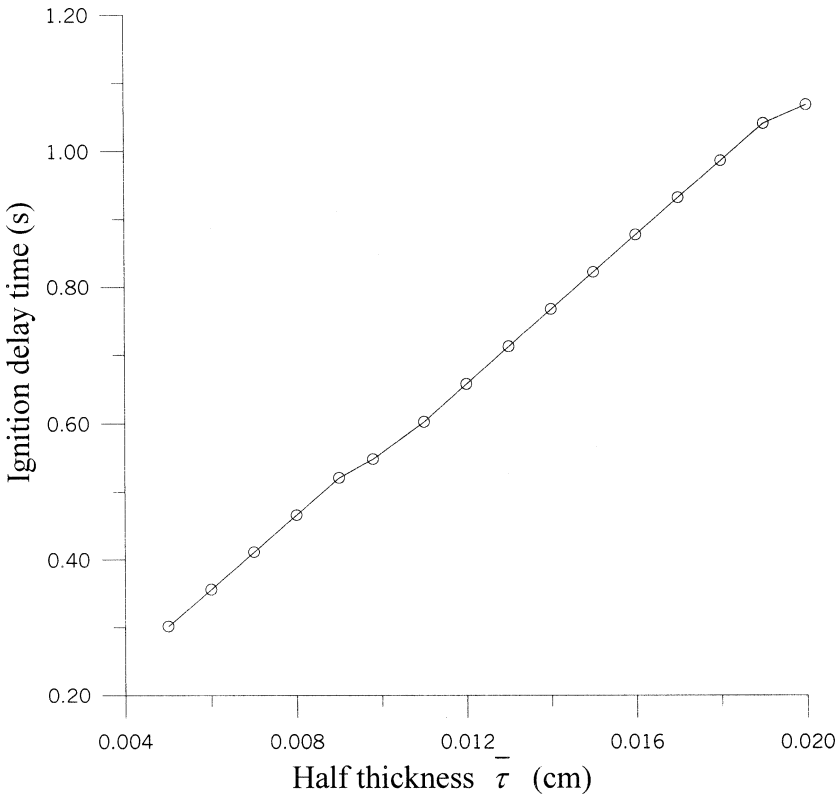

Figure 8. Ignition delay time as a function of solid-fuel thickness.

$\bar{T}_\infty = 298\,\mathrm{K}$. It can be seen that the predicted results are almost identical to this model and the one by Delichatsios (1986), except in the very thin regime. This discrepancy is due to finite-rate chemical kinetics. The flame chemistry was infinitely fast in Delichatsios' work (1986), whereas our model uses finite-rate kinetics. This factor $\pi/4$ arises from the exact solution of the problem. De Ris' $\sqrt{2}$ comes from an approximate solution; we expect the exact solution to be better.

The flame-spread rate was found to decrease with an inverse proportional to the solid-fuel thickness, and their relationship was found: $\bar{V}_\mathrm{f} = 0.013(\bar{\tau})^{-0.81}$. For a thinner solid fuel ($\bar{\tau} \leq 0.01\,\mathrm{cm}$), the flame-spread rate decreases faster than when $\bar{\tau} > 0.01\,\mathrm{cm}$. This trend coincides with the thermal theories of de Ris (1969) and experiments by

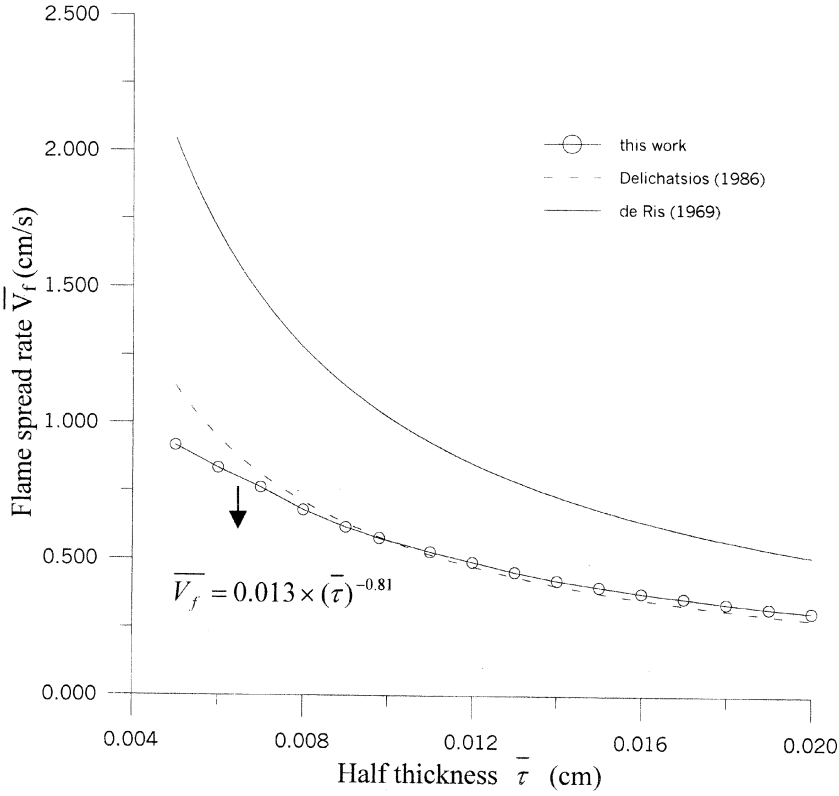

Figure 9. Flame-spread rate as a function of solid-fuel half-thickness.

Lastrina et al. (1971) and Suzuki et al. (1994). Note that the exponent, -0.81, on the thickness correlation is not the same as -1, which was predicted by de Ris (1969) and Delichatsios (1986). The reason is that the assumption of infinite-rate chemical kinetics is not still valid as fuel thickness decreases continuously (Di Blasi, 1994, 1995); in other words, the de Ris theory overpredicted the flame-spread rate for the thinner fuel.

Di Blasi (1994) used a steady combustion model to predict the flame-spread rate for various solid-fuel thicknesses. She categorized the thickness into three regimes: very thin, thin, and thick. In the thin regime, the spread rate also decreased as the solid-fuel thickness increased, as in this work.

The Effects of Changing Ambient Oxygen Concentration

Because the adiabatic flame temperature varies as the ambient oxygen concentration changes, the reference temperature changes as well, which leads to the variations in the thermodynamic properties. The reference velocity varies with the oxygen concentration as well, similar to changing the gravity level. Therefore, certain nondimensional parameter values (such as Da, A_s, τ, γ, etc.) are changed accordingly.

Figure 10 shows the ignition delay time as a function of the ambient oxygen concentration ($0.131 \leq Y_{O\infty} \leq 0.35$). The correlation between ignition delay time and ambient oxygen index is $t_{ig} = 0.854\, Y_{O\infty}^{-0.14}$. The ignition delay time is shortened as $Y_{O\infty}$ increases. Note that the variation in the ignition delay time is insignificant from 0.52 to 0.59 s within the aforementioned $Y_{O\infty}$ range. This is because the ignition delay time depends on the time required for the formation of a flammable mixture, and the heating process is independent of the ambient oxygen index. The trend of experimental result (Olson et al., 2001) is the same as that predicted by this study for $Y_{O\infty} \leq 0.35$.

Figure 11 shows the flame-spread rate versus the ambient oxygen concentration. The flame-spread rate is faster in a higher oxygen concentration environment; the chemical reaction rate is faster as $Y_{O\infty}$ increases, leading to a higher flame temperature. For example, $T_{max} \cong 10.0$ at $Y_{O\infty} = 0.35$, whereas $T_{max} \cong 6.0$ at $Y_{O\infty} = 0.15$. The predicted extinction limit is $Y_{O\infty} = 0.131$. The corresponding value obtained by Duh and Chen (1991), which used a steady combustion model, was $Y_{O\infty} = 0.132$. Sacksteder and T'iens' experiment (1994) found that the extinction limit is $Y_{O\infty} = 0.174$. The predicted extinction limit is lower than that obtained by the experiment because the gas-phase chemistry is described using a one-step global chemical reaction in the numerical model. Far from the extinction limit, the relationship between the flame-spread rate and the oxygen concentration is found to be $\bar{V}_f = 2.83\, Y_{O\infty}^{1.11}$ within the range of $0.18 \leq Y_{O\infty} \leq 0.35$. The experiment by Olson (1987) found that $\bar{V}_f \propto Y_{O\infty}^{1.18}$ for $Y_{O\infty} \geq 0.21$.

The Effects of Changing Incident Peak Heat Flux

Varying the incident peak heat flux corresponds to change in q_{ex}. This means that the total energy input to the solid fuel is changed because the Gaussian distribution half-width maintains the same profile. This parameter affects solid-phase pyrolysis.

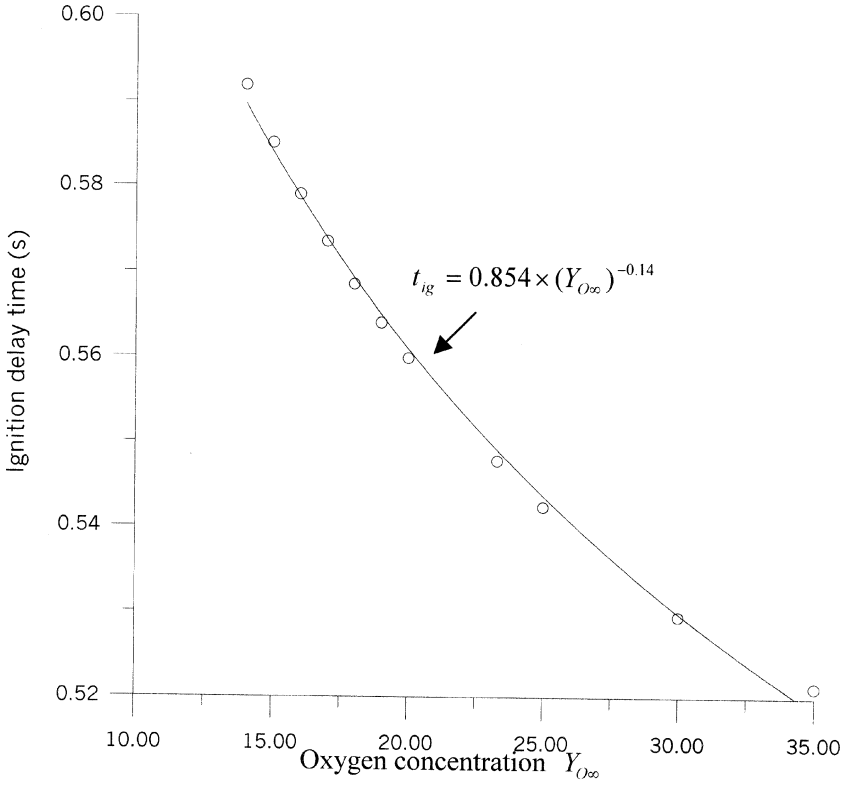

Figure 10. Ignition delay time varies with oxygen concentration.

Figure 12 displays the ignition delay time as a function of the incident peak heat flux, $2\,\mathrm{W/cm^2} \le \bar{Q}_{\max} \le 8\,\mathrm{W/cm^2}$, at $Y_{O\infty} = 0.233$ in the normal-gravity environment. It is obvious that the ignition delay time decreases as the incident peak heat flux increases. The major reason is associated with the formation time for the flammable mixture. The heat flux to the solid fuel is reduced as the incident peak heat flux decreases (half-width stays the same); meanwhile, the pyrolysis rate is reduced. Therefore, the flammable mixture formation time becomes longer. If the incident peak heat flux is less than $2\,\mathrm{W/cm^2}$, the solid-phase pyrolysis is still continuous but ignition is never initiated; therefore, it is impossible to have a spreading flame. The relationship between the ignition delay time and incident peak heat flux is $t_{\mathrm{ig}} = 3.31 \times (\bar{Q}_{\max})^{-1.11}$ within the range $2\,\mathrm{W/cm^2} \le \bar{Q}_{\max} \le 8\,\mathrm{W/cm^2}$. This result is similar to Mikkola and

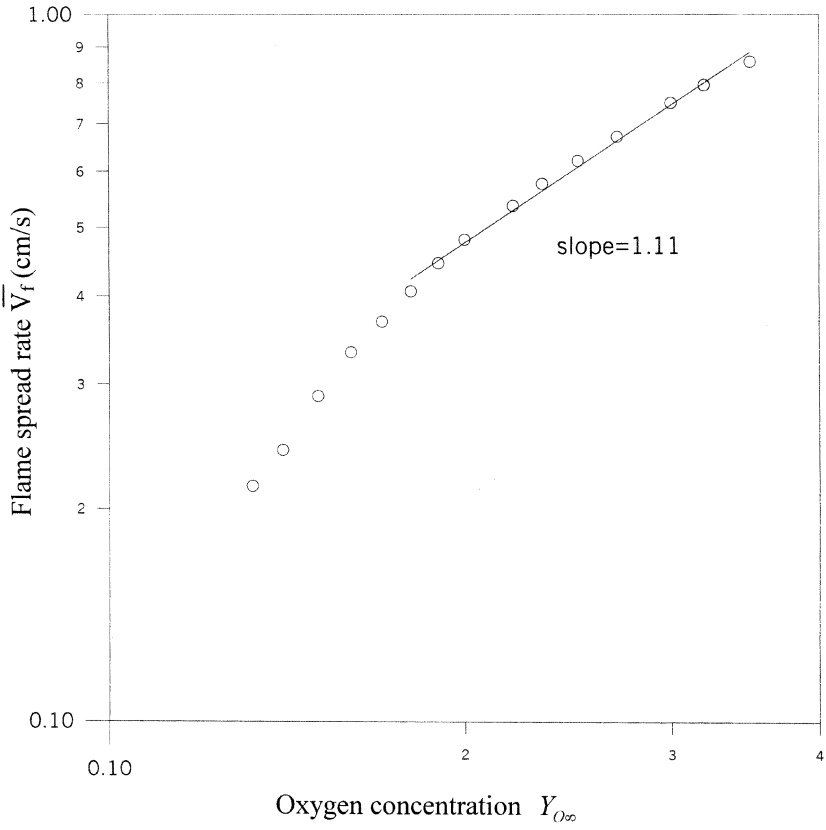

Figure 11. Flame-spread rate as a function of oxygen concentration.

Wichman's prediction (1989), which found $t_{ig} \propto (\bar{Q}_{max})^{-1}$ for a thermally thin fuel. The experiment by Babrauskas and Parker (1987) also observed this trend.

The steady flame-spread rate (0.576 cm/s) is independent of the incident peak heat flux. The influence of the incident peak heat flux on the flame behavior occurs only at the ignition period. In this period, all of the energy is received by the solid fuel from the incident radiant heat flux. When the flame is established and starts to spread, the incident heat flux no longer contributes to the solid-fuel pyrolysis. The upstream solid fuel receives energy from the flame via gas-phase conduction to generate the fuel vapor and from the flammable mixture for further continuous ignition upstream. The flame can now sustain itself.

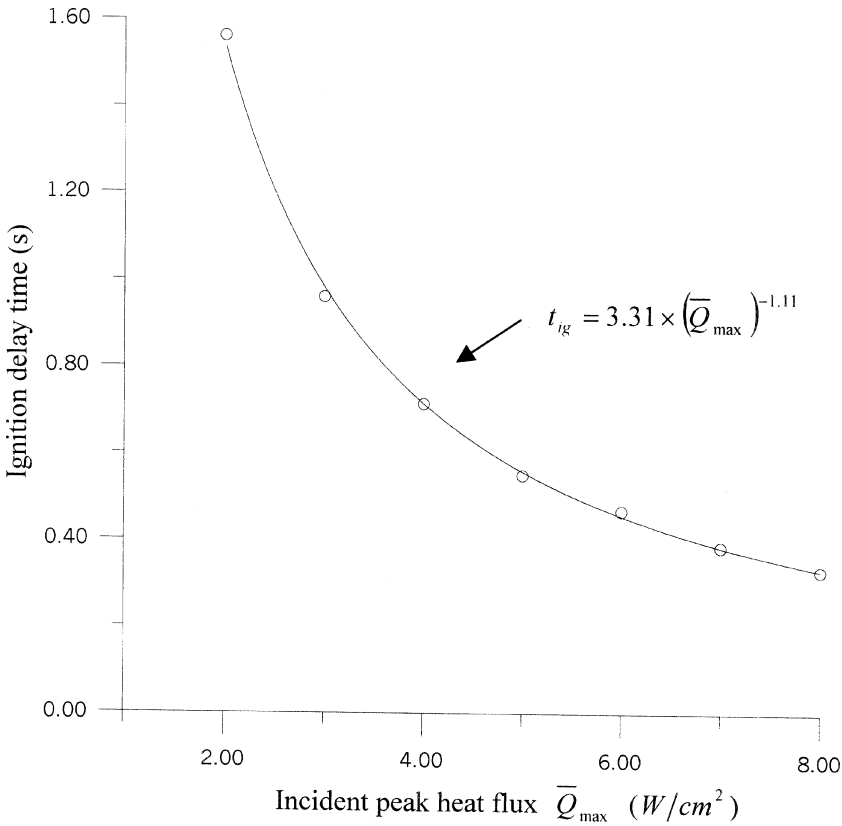

Figure 12. Ignition delay time varies with incident peak heat flux.

CONCLUSIONS

A numerical analysis was presented to study the ignition and subsequent downward flame spread over a thermally thin solid fuel in a gravitational field. The ignition and transition to flame-spread process can be described as follows. At the beginning of the heat-up stage ($0 \leq \bar{t} < 0.55$ s), the solid-fuel temperature rose gradually and pyrolysis was insignificant. The pyrolysis became more intense as time proceeded. Eventually a flammable mixture was formed in the neighborhood of the fuel plate. As the local gas-phase temperature became high enough, ignition ($\bar{t} = 0.55$ s) took place, which consisted of two stages. In the induction period ($0.55\,\text{s} \leq \bar{t} \leq 0.71$ s), the reactivity and temperature were reinforced by

one another. Thermal runaway ($0.71\,\mathrm{s} \leq \bar{t} \leq 0.74\,\mathrm{s}$) followed, which produced a premixed flame. The flame first expanded and then shrank. A transformation ($0.74\,\mathrm{s} \leq \bar{t} \leq 0.93\,\mathrm{s}$) from the premixed flame into a diffusion flame was identified. As the diffusion flame became established, the flame front extended upstream in order to further gasify the virgin fuel to generate more fuel vapors to support itself. As soon as burnout appeared ($\bar{t} = 2.87\,\mathrm{s}$), the steady flame-spread occurred with a spread rate of 0.576 cm/s.

A series of parametric studies was performed. The ignition delay times within the gravity levels, $0.5 \leq g \leq 6.7$, were found to be almost the same; this value is about 0.55 s. The ignition delay time was controlled mainly by the formation time for the flammable mixture and was independent of the gravity level (or induced flow velocity). The flame-spread rate was lowered as the gravity level became greater because the strength of the gas phase forward conduction was reduced. The flame is blown off when the gravity level reaches $6.7\,\bar{g}_e$. The ignition delay time increases nearly linearly with the solid-fuel thickness in the range $0.005\,\mathrm{cm} \leq \bar{\tau} \leq 0.02\,\mathrm{cm}$. Since thicker fuel requires more time to pyrolyze the fuel into vapor the ignition delay becomes longer. The flame-spread rate decreases with an increase in solid-fuel thickness. For a thinner solid fuel ($\bar{\tau} \leq 0.01\,\mathrm{cm}$), the flame-spread rate decreases faster than when $\bar{\tau} > 0.01\,\mathrm{cm}$. The computed flame-spread rates are nearly identical to those predicted by Delichatsios (1986), except in the very thin regime. The ignition delay time was shortened as the ambient oxygen index increased. However, the difference, from 0.52 to 0.59 s within the range of $0.131 \leq Y_{O\infty} \leq 0.35$, was insignificant. This is because the ignition delay time depends on the formation of a flammable mixture but not the component concentration of the mixture. The flame-spread rate becomes faster in a higher $Y_{O\infty}$ environment. The relationship between the flame-spread rate and the oxygen concentration was $\overline{V_f} = 2.83\,Y_{O\infty}^{1.11}$ for $0.18 \leq Y_{O\infty} \leq 0.35$. The corresponding exponent obtained experimentally by Olson (1987) was 1.18. The predicted extinction limit was $Y_{O\infty} = 0.131$, almost identical to the Duh and Chen (1991) steady model. The ignition delay time decreased when the incident peak heat flux increased. A higher incident peak heat flux allows the formation time for the flammable mixture to become shorter, leading to earlier ignition. While the incident peak heat flux is below $2\,\mathrm{W/cm^2}$, the ignition cannot occur even when surface pyrolysis is in progress. The relationship

between the ignition delay time and the incident peak heat flux is found to be $t_{ig} = 3.31 \times (\bar{Q}_{max})^{-1.11}$.

In a microgravity environment the radiation heat transfer mode plays an important role and should not be neglected. A one-step overall chemical reaction was found not to be appropriate near the extinction limit. Therefore, in order to make this combustion model more complete, the radiation effect and multistep chemical kinetics will be included to study flame behavior in microgravity environments in the future.

NOMENCLATURE

A_s	nondimensional preexponential factor for fuel pyrolysis, $\bar{A}_s\bar{\alpha}^*/\bar{V}_r^2$
$\bar{B}$	preexponential factor for gas-phase reaction ($cm^3/mols$)
C	specific heat ratio of the gas mixture to solid fuel, $\bar{C}_p/\bar{C}_s$
$\bar{C}_p$	specific heat for gas mixture (J/gK)
$\bar{C}_s$	specific heat for solid fuel (J/gK)
$\bar{D}$	specific diffusivity (cm^2/s)
Da	Damköhler number, $\bar{B}\bar{\rho}^*\bar{\delta}/\bar{V}_r$
E	nondimensional activation energy, $\bar{E}/\bar{R}\bar{T}_\infty$
f	stoichiometric oxidizer/fuel mass ratio
g	nondimensional gravitational acceleration, $\bar{g}/\bar{g}_e$
$\bar{g}_e$	Earth normal gravity (cm/s^2)
Gr	Grashof number, $\bar{g}(\bar{\rho}_\infty - \bar{\rho}_f)\bar{\delta}^3/\bar{\rho}^*\bar{\nu}^{*2}$
k_s	nondimensional solid-phase conductivity, $\bar{k}_s/\bar{k}^*$
L	nondimensional latent heat, $\bar{L}/\bar{C}_s\bar{T}_\infty$
Le	Lewis number, $\bar{\alpha}/\bar{D}$
m_s''	nondimensional mass flux, $\bar{m}_s''\bar{\alpha}^*/\bar{\rho}_{s\infty}\bar{V}_r^2\bar{\tau}$
P	nondimensional pressure, $(\bar{p} - \bar{p}_\infty)/\bar{\rho}^*\bar{V}_r^2$
Pr	Prandtl number, $\nu/\bar{\alpha}$
q	nondimensional heat of combustion per unit mass of fuel, $\bar{q}/\bar{C}_p\bar{T}_\infty$
q_{ex}	nondimensional external heat flux, $\bar{q}_{ex}\bar{\alpha}^*/\bar{\tau}\bar{\rho}_{s\infty}\bar{C}_s\bar{T}_\infty\bar{V}_r^2$
Q_{ex}	nondimensional peak external heat flux
$\bar{R}$	universal gas constant (J/mol K)
t	nondimensional time, $\bar{t}\bar{V}_r^2/\bar{\alpha}^*$
T	nondimensional gas-phase temperature, $\bar{T}/\bar{T}_\infty$
T_s	nondimensional solid-phase temperature, $\bar{T}_s/\bar{T}_\infty$

u	nondimensional velocity parallel to the fuel surface, $\bar{u}/\bar{V}_r$
v	nondimensional velocity normal to the fuel surface, $\bar{v}/\bar{V}_r$
$\bar{V}_r$	reference velocity, $[\bar{g}(\bar{\rho}_\infty - \bar{\rho}_f)\bar{\alpha}^*/\bar{\rho}^*]^{1/3}$
$\bar{V}_f$	flame-spread rate (cm/s)
x	nondimensional distance parallel to the fuel surface, $\bar{x}/\bar{\delta}$
x_{bo}	burnout position
y	nondimensional distance normal to the fuel surface, $\bar{y}/\bar{\delta}$
Y_F	fuel mass fraction
Y_O	oxygen mass fraction

Greek Symbols

$\bar{\alpha}$	thermal diffusivity (cm^2/s)
β	Gaussian distribution shape factor
γ	temperature ratio, $\bar{T}^*/\bar{T}_\infty$
$\bar{\delta}$	reference length (cm)
μ	nondimensional dynamic viscosity, $\bar{\mu}/\bar{\mu}^*$
$\bar{\nu}$	kinematic viscosity (cm^2/s)
ρ	nondimensional density of gas phase, $\bar{\rho}/\bar{\rho}^*$
ρ_s	nondimensional density of solid phase, $\bar{\rho}_s/\bar{\rho}_{s\infty}$
$\bar{\tau}$	solid fuel half thickness (cm)
$\dot{\omega}_F$	nondimensional gas-phase reaction rate, $-Da\,\rho^2 Y_F Y_O \exp(-E/T)$

Superscript

$''$	flux
$*$	reference state
–	dimensional quantities

Subscript

ex	external
F	gaseous fuel
max	location of downstream boundary
min	location of upstream boundary
O	oxizider
s	solid phase
sf	burnout state
∞	ambient condition

REFERENCES

Altenkirch, R.A., Eichhorn, R., and Shang, P.C. (1980) Bouyancy effects on flames spreading down thermally thin fuels. *Combust. Flame*, **37**, 71–83.

Babrauskas, V. and Paker, W.J. (1987) Ignitability measurements with the cone calorimeter. *Fire Mater.*, **11**, 31–43.

Chen, C.H. and Cheng, M.C. (1994) Gas-phase radiative effects on downward flame spread in low gravity. *Combust. Sci. Technol.*, **97**, 63–83.

Chen, C.H. and Hou, W.H. (1991) Diffusion flame stabilization and extinction under naturally convective flows. *Combust. Flame*, **83**, 309–324.

Delichatsios, M. (1986) Exact solution for the rate of creeping flame spread over thermally thin materials. *Combust. Sci. Technol.*, **44**, 257–267.

de Ris, J.N. (1969) Spread of a laminar diffusion flame. *Proc. Combust. Instit.*, **12**, 241–252.

Di Blasi, C. (1994) Processes of flames spreading over the surface of charring fuels: Effects of the solid thickness. *Combust. Flame*, **97**, 225–239.

Di Blasi, C. (1995) Predictions of wind-opposed flame spread rates and energy feedback analysis for charring solids in a microgravity environment. *Combust. Flame*, **100**, 332–340.

Duh, F.C. and Chen, C.H. (1991) A theory for downward flame spread over a thermally thin fuel. *Combust. Sci. Technol.*, **77**, 291–305.

Ferkul, P.V. and T'ien, J.S. (1994) A model of low-speed concurrent flow flame spread over a thin fuel. *Combust. Sci. Technol.*, **99**, 345–370.

Fernandez-Pello, A.C. and Hirano, T. (1983) Controlling mechanisms of flame spread. *Combust. Sci. Technol.*, **32**, 1–31.

Jiang, X. and Fan, W.C. (1995) Numerical prediction of flame spread over solid combustibles in a microgravity environment. *Fire Safety J.*, **24**, 279–298.

Kashiwagi, T. (1982) Effects of sample orientation on radiative ignition. *Combust. Flame*, **44**, 223–245.

Kashiwagi, T., McGrattan, K.B., Olson, S.L., Fujita, O., Kikuchi, M., and Ito, K. (1996) Effects of slow wind on localized radiative ignition and transition to flame spread in microgravity. *Proc. Combust. Instit.*, **26**, 1345–1352.

Lastrina, F.A., Magee, R.S., and McAlevy, R.F., III. (1971) Flame spread over fuel beds: Solid-phase energy considerations. *Proc. Combust. Instit.*, **13**, 935–948.

Lin, T.H. and Chen, C.H. (1999a) Influence of two-dimensional gas phase radiation on downward flame spread. *Combust. Sci. Technol.*, **141**, 83–106.

Lin, T.H. and Chen, C.H. (1999b) Numerical analysis of ignition and transition to downward flame spread over a thermally thin solid fuel. *Int. J. Trans. Phenomena*, **1**, 255–275.

McGrattan, K.B., Kashiwagi, T., Baum, H.R., and Olson, S.L. (1996) Effects of ignition and wind on the transition to flame spread in a microgravity environment. *Combust. Flame*, **106**, 377–391.

Mikkola, E. and Wichman, I.S. (1989) On the thermal ignition of combustible materials. *Fire Mater.*, **14**, 87–96.

Nakabe, K., McGrattan, K.B., Kashiwagi, T., Baum, H.R., Yamashita, H., and Kushida, G. (1994) Ignition and transition to flame spread over a thermally thin cellulosic sheet in a microgravity environment. *Combust. Flame*, **98**, 361–374.

Nakamura, Y., Yamashita, H., Takeno, T., and Kushida, G. (2000) Effects of gravity and ambient oxygen on a gas-phase ignition over a heated solid fuel. *Combust. Flame*, **120**, 34–48.

Olson, S.L. (1987) *The Effect of Microgravity on Flame Spread over a Thin Fuel.* NASA TM-100195.

Olson, S.L. (1991) Mechanisms of microgravity flame spread over a thin solid fuel: Oxygen and opposed flow effects. *Combust. Sci. Technol.*, **76**, 233–249.

Olson, S.L., Ferkul, P.V., and T'ien, J.S. (1988) Near-limit flame spread over a thin solid fuel in microgravity. *Proc. Combust. Instit.*, **22**, 1213–1222.

Olson, S.L., Kashiwagi, T., Fujita, O., Kikuchi, M., and Ito, K. (2001) Experimental observations of spot radiative ignition and subsequent three-dimensional flame spread over thin cellulose fuels. *Combust. Flame*, **125**, 852–864.

Parker, W.J. (1972) Flame spread model for cellulosic materials. *J. Fire Flammability*, **3**, 254–269.

Patankar, S.V. (1980) *Numerical Heat Transfer and Fluid Flow*, McGraw–Hill, New York.

Sacksteder, K.R. and T'ien, J.S. (1994) Buoyant downward diffusion flame spread and extinction in partial-gravity accelerations. *Proc. Combust. Instit.*, **25**, 1685–1692.

Suzuki, M., Dobashi, R., and Hirano, T. (1994) Behavior of fires spreading downward over thick paper. *Proc. Combust. Instit.*, **25**, 1439–1446.

Tewarson, A. and Ogden, S.D. (1992) Fire behavior of polymethylmethacrylate. *Combust. Flame*, **89**, 237–259.